Supporting Information

Size-tailorable Lignin Nanoparticle Synthesis: Effects of Solution Chemistry and DLVO Forces on Amphiphilic Balance of Lignin

Qianwei Li [a], Hanwen Zhang [a], Jaewon Lee [b, *], Caixia Wan [a, *]

[a] Department of Biomedical, Biological, and Chemical Engineering, University of Missouri, 1406 East Rollins Street, Columbia 65211, USA
[b] Department of Mechanical and Aerospace Engineering, University of Missouri, 416 South 6th Street, Columbia 65211, USA
[*]Corresponding author. Tel: +1 573 884 8918; E-mail: j.lee@missouri.edu. Tel: +1 573 884 7882; E-mail: wanca@missouri.edu.

Number of Pages: 22
Number of Tables: 2
Number of Figures: 11

Table of Content

Supplemental experimental section

Materials

Kraft lignin was kindly provided by Domtar Cooperation (Fort Mills, South Carolina) and dried at 100 ℃ for 4 h prior to use. Organosolv lignin was supplied by Attis Industries, Inc. All the chemicals were purchased from Fisher Scientific (Waltham, MA) and used as received.

Preparation of kraft lignin fractions

Ethanol-water (95:5, v/v) or acetone-water (30:70, v/v) was used for the fractionation of kraft lignin. Kraft lignin and organic solvent-water were mixed at the mass ratio of 1:3 and stirred for 3 h at room temperature. The mixture was then centrifuged at 5000 rpm for 10 min to separate the solvent-soluble and insoluble fractions. The solvent-insoluble fraction was washed with the same solvent three times, and the supernatant was combined with the soluble fraction. The collected soluble fraction from the ethanol-water fractionation, denoted as EKL, was vacuum evaporated to remove ethanol, freeze-dried, and stored in a desiccator prior to further use. The collected insoluble fraction from the acetone-water fractionation, denoted as AKL, was freeze-dried and stored in a desiccator prior to further use.

Characterization of lignin and lignin nanoparticles

Gel permeation chromatography (GPC) was used to quantify the molecular weight distribution of lignin. Before the GPC measurement, lignin was acetylated by reacting with 1:1 acetic anhydride/pyridine at 80 ℃ overnight. All the acetylated lignin can be directly dissolved in the mobile phase tetrahydrofuran (THF) at 2 mg/mL. The analysis was performed using an Agilent HPLC instrument equipped with a RID detector and an Agilent PLgel 5 μm MIXED-D column S5 (300×7.5 mm). Both refractive index detector (RID) and column temperatures were maintained at 35 °C. THF was a mobile phase, eluting at 1 mL/min. Polystyrene standards (MW 250-70000) were used as standards for calibration. Transmission electron microscopy (TEM) imaging was performed on a JEOL-2100FFEI Tecnai G2 F30 300 kV microscope. The samples for the imaging were prepared by dropping 5 μL of 0.2 wt% LNP suspension onto the 200-mesh carbon-coated copper TEM grid. The size distribution and ζ potential of LNPs were measured by dynamic light scattering (DLS) with the scattering angle of 90° (Malvern Instruments, Malvern, UK). The functional group contents in lignin were quantified by ^{31}P NMR on a Bruker AVIII 800 MHz spectrometer following a reported protocol.[1]

UV ionization difference method

The ionizable phenolic hydroxyl groups of lignin were measured by UV difference method previously reported.[2] The buffer (pH 12) was prepared by dissolving 1.55 g of boric acid with 100 mM NaOH solution to reach a final volume of 250 mL, and the buffer (pH 6) was prepared by mixing 61.875 mL of 200 mM KH_2PO_4, 14.125 mL of 100 mM NaOH, and a certain amount of DI water to reach a final volume of 500 mL. Lignin solution (5 mg/mL) in 68 wt% acetone was prepared as a stock solution. The stock solution was then diluted using 68 wt% acetone to a final lignin concentration of 500, 1000, 2000, and 5000 ppm as working solutions. The working lignin solutions were mixed with pH 6 buffer, pH 12 buffer, 200 mM NaOH solution, or 20 mM NH_4HCO_3 to the final lignin concentration of 50 ppm. The wavelength of the UV spectrum scanning was 190-400 nm. The closest values to NMR data were achieved at 14.1 g/L for KL and 28.2 g/L for both OL and EKL. It suggests that the phenolic hydroxyl groups in KL tend to expose and easily ionize under a hydrophilic condition while OL and EKL chains have a better expansion at high acetone concentrations. However, excessive acetone can cause a negative impact on the measurement due to the reduction in salt solubility in the acetone solution.

Estimation of initial particle separation distance

$$D_{average} = 2R_{cell} = 2 \times \left(\frac{3M_w}{4\pi N_A \rho_{mixture} c_{lignin}}\right)^{\frac{1}{3}} \quad (S1)$$

Where M_w is the weight average molecular weight of lignin (g/mol), $\rho_{mixture}$ is the density of water (kg/m^3), and c_{lignin} is the initial lignin concentration (kg/kg). The calculation of the average particle distance is based on the cell model.[3]

Estimation of area per ionizable group based on a single lignin chain

The dissociation constants for these groups can vary from different structures of lignin, but they were assumed to be constant in this study, where pK_a = 4.8 for the carboxylic group acid and pK_a = 10.2 for the phenolic hydroxyl group.[4] The ionizable phenolic hydroxyl group can be further classified into Type I and Type II.

As the first attempt to estimate the average area per ionizable group on the surface, it was based on the following assumptions: 1) lignin molecule with the average molecular weight of $M_{w,\,GPC}$ (measured by GPC) has the ionizable group content of c_{NMR} (measured by ^{31}P NMR). This information can be used as a representative over the lignin molecule population; 2) all the ionizable groups locate on the surface to contribute to the electrostatic repulsive force in particle-particle interaction; 3) Different ionizable groups share the same possibility to present on the surface. The area per ionizable group (S) is used to quantify the surface chemistry of nanoparticles in the electrostatic force calculation. S describes the distribution of the ionizable groups on the surface of lignin particles and can be calculated with the surface area per particle and the number of ionizable groups on the surface ($N_{surface}$). The ratio of $S_{PeOH,\,10.2}$ /$S_{PeOH,\,7.5}$, and $S_{PeOH,\,10.2}$ /S_{COOH} would maintain same for the same lignin type in the following calculation based on the above assumptions.

$$S = \frac{4\pi R^2}{N_{surface}} = a\frac{4\pi R^2}{M_w c_{surface}} \quad (S2)$$

M_w is the weight average molecular weight of lignin or LNPs (g/mol); $c_{surface}$ is the concentration of the ionizable groups on the particle surface (mol/g lignin), which is the function of M_w.

The number of functional groups $N_{surface}$ can be calculated by multiplying the mole concentration of the functional groups $c_{surface}$ with M_w of LNPs. Assuming that one lignin molecule forms one particle and all the ionizable groups are exposed on the surface, $c_{surface}$ can be approximated to c_{NMR} and $M_{w,\,GPC}$. However, it should be noted that both the particle radius and the functional group content are related to M_w of the lignin fragment. In the estimation of the particle radius, a mathematic correlation between the radius of gyration R_{gyr} and the molecular weight of lignin molecules obtained from a molecular dynamics study was used.[5] In this study, this correlation was found to not be sensitive to the lignin source, thus the parameters for spruce lignin were selected.

$$R_{gyr}(M) = 6.085(0.001M)^{0.361}(\text{Å}) \quad (S3)$$

Based on this equation, the particle size of the lignin fragment with M_w 580 to 27008 (which covers above 90 % of KL based on the GPC data) ranges from 1 to 4 nm. It gives the surface area on the numerator of the calculation about one order increase, while the denominator can be at least two order increase. The number of phenolic groups was shown linearly proportional to M_w of lignin fragment.[6] For example, the number of phenolic hydroxyl groups in the lignin fragment with Mw 12000 g/mol is approximately 2.25 times the phenolic hydroxyl groups in the lignin fragment of M_w 4000 g/mol. In summary, the *S* is likely to be overestimated using the measured average values if the lignin fragment with higher molecular weight is preferred in the actual self-assembly. A correction method to estimate *S* will be

discussed in the next section.

Estimation of area per ionizable group based on nanoparticle size

In the particle size prediction, we further calibrate the area per ionizable group based on the following assumptions. First, the availability of the ionizable group on the particle surface depends on the hydrophilicity of lignin and the solution chemistry. The plausible S_{COOH} should vary based on the lignin type and pH of the mixture. Secondly, a smaller interparticle distance can increase the collision efficiency and lignin chains would attach before extending to a structure with more ionizable groups on the surface, especially at a high lignin concentration. At the concentration range before the rapid precipitation occurrence, the surface ionizable group density of lignin particles is mainly determined by the first assumption. The tuning effect of the solution pH on the lignin structure is limited with the same antisolvent, it leads to a similar surface ionizable group density. Thus, a calibration point was picked from the data based on medium lignin concentrations for the prediction under weak acid conditions to estimate the possible exposure of ionizable groups on LNP surface. In the DLVO-PBE modeling, the average particle size is derived from the energy profile of the interparticle interaction. Using the calibration point from experimental data can reversely calculate the S_{COOH} of the particles. First, the pH and salt concentration of the calibration point were applied in the calculation. Then, the calculated average particle size was plotted as the function of a certain range of S_{COOH} values. The measured particle size of the calibration point was used to find the corresponding S_{COOH} via interpolation. The found S_{COOH} can represent the distribution of average ionizable groups on the surface for the LNPs. Using the calibration point, it is assumed that at a certain pH range, the lignin structure as well as the inner molecular interaction such as hydrogen bonding and π-π stacking were not interrupted significantly due to the similar dissociation degree of the phenolic groups.

Calculation of interaction force

van der Waals energy

The plate–plate energy for van der Waal (E_{PP}^{vdw}):

$$E_{PP}^{vdw}(D) = -\frac{A}{12\pi D^2} \quad (S5)$$

Electrostatic double-layer force

The charge-regulation model by Ninham and Parsegian[7] in the calculation of the F_{PP}^{elec} is selected because a classic DLVO theory with an assumption of constant charge or constant potential is insufficient at a small distance. This charge-regulation model considers the density of the ionizable groups on the surface and their degree of dissociation at various pH values in the calculation of the electric double-layer force. The reduced potential at the center between two plates is converted from the full potential as:

$$\xi = e^{e\beta\psi(0)} \quad (S6)$$

ξ or $\psi(0)$ is determined by the average surface area per ionizable group (S), the dissociation constant of the ionizable group (Z), the hydrogen ion concentration (H), and the separation distance b (=D/2). The analytical expression (**Table S2**) of ξ is determined by the distance range in which the b falls and whether ξ is larger than $\frac{1}{\sqrt{2}}$. The distance between two plates can be divided into three conditions: C1) $b < \frac{1}{\kappa}$ where ξ is independent on the screening effect and falls to zero rapidly; C2) $\frac{1}{\kappa} \leq b \leq \frac{\pi}{\kappa}$ where ξ is mainly contributed by the decay length κ (= $(\frac{8\pi n e^2}{k_B T \varepsilon})^{\frac{1}{2}}$) and b with trivial perturbation from the dissociation of ionizable groups; and C3)

$b > \frac{\pi}{\kappa}$ where $\psi(0)$ is approximated to zero. In C1 and C2, ξ is smaller than $\frac{1}{\sqrt{2}}$, while in C3, ξ should be larger than $\frac{1}{\sqrt{2}}$, indicating that the potential is approximately 0.

The distance-based ξ can cause discontinuity in the full force curve between the ranges (e.g., from 0 to 100 nm). To generate a smooth force curve, the discontinuous section between the C1 and C2 boundary was selected and smoothed using linear interpolation (python function **UnivariateSpline**). The fitted data were only applied on the distance ranging from $\frac{1}{\kappa} - 2$ to $\frac{1}{\kappa} + 2$ angstroms. The interaction forces for different functional groups were calculated separately and were added up as the total electrostatic force. The total force curve is used to find the potential energy of plate-plate interaction via integral (python function **simps**). The schematic of the calculation and the example of the force curve are shown in Figure S10.
Based on the definition, ζ is the reduced potential of the middle of two plates. With ξ, the surface potential can be obtained via:

$$\Psi_{PP}^{elec}(D) = \frac{k_B T}{e}[\ln \Phi(D) + \ln \xi] \quad (S7)$$

$\Phi(D)$ is written below with an elliptic function cd (calculated via the python function **ellipfun** ('cd', u=u, m=k^2)). b in the equation for u is half of the separation distance D as previously mentioned. The data smoothness for electric double-layer potential follows the same procedure as in the force calculation after the selection of the valid ξ at each distance point.

$$\Phi(D) = \Phi(-) + [1 - \Phi(-)]cd^2(u;k) \quad (S8)$$

$$\Phi(\pm) = \frac{\left\{(1-\eta) + \frac{\eta}{2\xi} \pm \sqrt{\left[(1-\eta) + \frac{\eta}{2\xi}\right]^2 + 2\eta\xi}\right\}}{2\xi^2} \quad (S9)$$

$$u = \frac{\kappa \xi^{\frac{1}{2}} b}{2}\left(\frac{\sqrt{\left[(1-\eta) + \frac{\eta}{2\xi}\right]^2 + 2\eta\xi}}{\xi^2}\right)^{\frac{1}{2}} \quad (S10)$$

$$k^2 = \frac{[1 - \Phi(-)]\xi^2}{\sqrt{\left[(1-\eta) + \frac{\eta}{2\xi}\right]^2 + 2\eta\xi}} \quad (S11)$$

Sphere-sphere interaction energy

The plate-plate interaction force is further applied in the interaction between lignin spherical particles via Derjaguin approximation (Figure S11).

$$F_{SS} = 2\pi R_{eff} E_{PP} \quad (S12)$$

R_{eff} $(= \frac{r_i r_j}{r_i + r_j})$ is the effective radius of two spheres with the radius of r_i and r_j. Let $r_i < r_j$. E_{PP} is the interaction energy of the plate–plate force. The sphere-sphere potential can be obtained numerically via the following:[8]

$$\mathrm{E}_{SS}(\varepsilon) = E_{SS,1} - E_{SS,2} - E_{SS,3} + E_{SS,4} \quad (S13)$$

$$E_{SS,1} = 2\pi \int_0^{r_i} r \sqrt{1 - \frac{r^2}{r_j^2}}\, \mathrm{E}_{PP}\left(D_{ss} - r_i\sqrt{1 - \frac{r^2}{r_i^2}} - r_j\sqrt{1 - \frac{r^2}{r_j^2}}\right) dr \quad (S14-1)$$

$$E_{SS,2} = 2\pi \int_0^{r_i} r \sqrt{1-\frac{r^2}{r_j^2}}\,\mathrm{E}_{PP}\left(D_{ss} + r_i\sqrt{1-\frac{r^2}{r_i^2}} - r_j\sqrt{1-\frac{r^2}{r_j^2}}\right)dr \qquad (S14-2)$$

$$E_{SS,3} = 2\pi \int_0^{r_i} r \sqrt{1-\frac{r^2}{r_j^2}}\,\mathrm{E}_{PP}\left(D_{ss} - r_i\sqrt{1-\frac{r^2}{r_i^2}} + r_j\sqrt{1-\frac{r^2}{r_j^2}}\right)dr \qquad (S14-3)$$

$$E_{SS,4} = 2\pi \int_0^{r_i} r \sqrt{1-\frac{r^2}{r_j^2}}\,\mathrm{E}_{PP}\left(D_{ss} + r_i\sqrt{1-\frac{r^2}{r_i^2}} + r_j\sqrt{1-\frac{r^2}{r_j^2}}\right)dr \qquad (S14-4)$$

It is noted that unlike the case of planar where D is the distance between the surface of the planar, D_{ss} is the distance between the center of two spheres. For simplicity, a normalized distance between two spherical particles $r_i,\ r_j$ $(r_i < r_j)$ is used in the following calculation.

$$\varepsilon = \frac{D_{ss} - (r_i + r_j)}{r_i + r_j} = \frac{D_{PP}}{0.5(r_i + r_j)} \qquad (S15)$$

We can also find that $\delta D_{ss} = \delta D_{PP} = 0.5(r_i + r_j)\delta\varepsilon$. Let a denote as the radius ratio r_j/r_i. For van der Waals force, the exact solutions from above are expressed as:

$$\mathrm{E}_{SS}^{vdw}(\varepsilon) = \frac{A}{6}\left[\frac{2a}{2(1+a)\varepsilon + \varepsilon^2} + \frac{2a}{\varepsilon^2 + 2a\varepsilon + 4a} + ln\frac{\varepsilon^2 + 2(a+1)\varepsilon}{\varepsilon^2 + 2(1+a)\varepsilon + 4a}\right] \qquad (S16)$$

Population balance model

This population balance model can be solved numerically by the fixed pivot technique in which the particle volume is divided into 64 classes as:[9]

$$\frac{dn_k}{dt} = \sum_{\substack{i+j=k \\ v_{i-1}\le(v_i=v_k)\le v_{i+1}}} \left(1 - \frac{1}{2}\delta_{i,j}\right)\eta\beta_{ij}n_i n_j - n_k\sum_{i=1}^{64}\beta_{ik}n_i \qquad (S17)$$

where β_{ij} is an aggregation kernel, k is the class number; $\delta_{i,j}$ is the Kronecker delta and equals 1 when $j = k$ and 0 otherwise. The volume bin size is 1.5 times the initial particle volume after optimization. η is used to preserve numbers and mass and is given by.

$$\eta = \begin{cases} \dfrac{v_{i-1} - (v_j + v_k)}{v_{i+1} - v_i}, v_i \le (v_j + v_k) \le v_{i+1} \\ \dfrac{(v_j + v_k) - v_{i-1}}{v_i - v_{i-1}}, v_{i-1} \le (v_j + v_k) \le v_i \end{cases} \qquad (S18)$$

The aggregation kernel β_{ij} is obtained as:

$$\beta_{ij} = \frac{2k_B T}{3\mu W_{ij}}(r_i + r_j)\left(\frac{1}{r_i} + \frac{1}{r_j}\right) \qquad (S19)$$

$$W_{ij} = \left(1 + \frac{r_j}{r_i}\right)\int_0^{\infty} \frac{\exp\left(\frac{\mathrm{E}_{SS}}{k_B T}\right)}{\mathrm{G}\left(\varepsilon, \frac{r_j}{r_i}\right)(\varepsilon+2)^2}\,(r_j > r_i) \qquad (S20)$$

$G\left(\varepsilon, r_j/r_i\right)$ is the term which takes the viscous interactions between particles into account and depends on the distance between two particles and the radius ratio over the two collision particles. $\varepsilon\left(=\frac{D-(r_i+r_j)}{r_i+r_j}\right)$ is the normalized separation distance. To save the computational cost, the W_{ij} was first calculated for a series of r_i with the r_j/r_i ranging from 1 to 5 times. Then, the

data were used to interpolate the W_{ij} for different r_i in the population balance model (python function interp1d (kind = 'quadratic')). It was observed that there is a good quadratic relationship between r_i and $ln(W_{ij})$, thus the interpolation is sufficient for the calculation.

Supplementary results

Effects of functional groups on electrostatic force calculation

Three methods, M0, M1, and M2 were used to identify the contribution of phenolic groups with different pK_a to the electrostatic force, and the S calculated from the above method for KL was used. M0 is the case where only the ionization of the carboxylic groups was considered. In M1, phenolic groups were divided into two groups, i.e., pK_a 7.5 and pK_a 10.2, and the content of PeOH with the pK_a 7.5 was estimated from the UV difference measurement (Table S3). The ionization degree of both the phenolic hydroxyl and carboxylic acid groups in 20 mM NH_4HCO_3 solution was first calculated based on the following equation. The dissociation degree is 0.7152 for phenolic hydroxyl groups with pK_a 7.5 and 0.9992 for carboxylic acid groups. The total ionizable group content was calculated by dividing the ionized content from UV measurements by the corresponding dissociation degree. The phenolic group content with pK_a 10.2 was found by subtracting the low dissociation constant from the total content. In M2, all the phenolic groups have the same pK_a10.2. The area per ionizable group for M1 and M2 is listed in Table S1.

$$\alpha_{ionizable\ group} = \frac{K_{a,ionizable\ group}}{K_{a,ionizable\ group} + 10^{-pH}} \quad (S4)$$

Where $K_{a,ionizable\ group}$ is the dissociation constant of the ionizable group, and pH is the bulk pH of the solution. The pH of 20 mM NH_4HCO_3 is 7.9.

Three pH levels of 3.63, 5.3, and 7.3 were used first to demonstrate the differences among the three calculation methods of the energy contribution of ionizable groups with various dissociation constants (Figure S7). Overall, the interaction between two particles of identical size would have a more profound energy barrier when M1 was used due to a higher dissociation degree for the phenolic group with pK_a 7.5. As the pH approaches neutral or higher, the energy gap becomes slightly larger from M0, M2, to M1. In the pH range of 5.3 to 7.3, the dissociation degree of the carboxylic groups can approximate 1, and the phenolic groups with lower pK_a would have relatively more contribution to the repulsive force. The dissociation degree $\alpha_{PeOH,7.5}$ increases from 0.026 to 0.387 while $\alpha_{PeOH,10.2}$ remains in the order of 10^{-4} to 10^{-3}. Meanwhile, the energy depth of the particle interaction can reach a much deeper level even for small particles as the pH increases from 5.3 to 7.3, along with more concentration from the ionization of the phenolic groups. However, when the separation distance between two particles gets smaller at a pH level close to neutral or higher, the $pH_{surface}$ drops significantly, leading to the re-protonation of the ionizable groups due to the charge regulation effect. Given the high dissociation constant of phenolic groups, it can be expected that such an ionizable group cannot contribute to the repulsive force in particle-particle interaction either at a small distance or in the pH around 5.3 or lower. The stability of the LNPs in DI water would more likely rely on the carboxylic groups on the surface. In all, M1 is selected in the following calculation as it includes more factors that help build up the energy barrier of the particles. From the initial estimation of S_{COOH} based on NMR data, OL-LNPs should achieve a sufficient energy barrier in a smaller size than KL-LNPs. This inference disagreed with the experimental observations, suggesting that the size determination does not directly relate to the overall carboxylic group content, but other structural properties of lignin would play a role in the arrangement of carboxylic groups on the surface.

Measurement of phenolic hydroxyl groups via ionization UV difference method

In the UV difference measurement, the detectable ionized phenolic hydroxyl content varied at different acetone concentrations (Figure 1a and S2). As a control, the total phenolic hydroxyl group content was also measured and compared with NMR data. The closest values of the standard UV difference measurement to NMR data were achieved at 14.1 g/L for KL and 28.2 g/L for both OL and EKL (Figure 1a). OL had the most ionizable phenolic hydroxyl groups, including the dominant Type I and minor Type II. Only Type I was detected in EKL, and ionization of phenolic structures was minor in KL. On the other hand, the absorbance difference at different acetone concentration suggests that the ionization of phenolic hydroxyl groups in lignin is not only determined by the pH but also the lignin solubility in the solution, leading to a distinguishable lignin structure. The ionized phenolic hydroxyl groups content in 20 mM NH_4HCO_3 as the function of acetone concentration was shown in Figure 1b. Interestingly, the measured phenolic hydroxyl groups in OL increase as the acetone concentration reduces. The corresponding ionization difference spectrum of OL (Figure S3b) shows a hypsochromic shift from an acetone concentration of 56.4 to 5.6 g/L suggesting that π-π stacking in lignin is altered. The absorbance at the same lignin concentration increases with less acetone in the solution, indicating that lignin chains become more "folded" with strong π-π stacking interaction. The increase in ionized phenolic hydroxyl groups along with the alteration of π-π stacking of OL is reckoned as the tunning effect of the weak base antisolvent on LNPs production. The spectrum of EKL also has the bathochromic shift, but that of KL does not. While both EKL and KL have a more complicated relationship between the π-π stacking interaction and the acetone concentration, further fundamental studies would be needed to have better insights into the role of different phenolic hydroxyl groups in the lignin conformation.

Estimation of S_{COOH} for DLVO-PBE model

A supplementary assumption for DLVO-PBE model is the relation between the exposure of ionizable groups on the particle surface and lignin structure. The calculation of the monomer size and surface ionizable group density can be calculated explicitly when the monomer is a single lignin chain. However, the direct estimation of the surface ionizable group density for the F^{elec} calculation gets complicated as more chains attach. Instead of estimation based on the properties of a single lignin chain determined by NMR and GPC, the ionizable group density is estimated based on the size of the formed particles. Thus, a calibration point (marked asterisk in Fig. 6a-d) was picked to estimate the relation among particle volume, number of monomers, and charged group density of the aggregates. The calibration point is one of the data points for synthesis using the same antisolvent and lignin source in the following size prediction. At the low pH range, the initial lignin concentrations of 10 and 3 g/L were selected for KL and OL, respectively, to estimate the S_{COOH}, and thus the LNP size at other initial concentrations can be predicted based on the DLVO-PBE model by assuming the self-assembly of lignin chains are similar at a certain pH range (e.g., weak acid, weak base) and for the same type of lignin. For example, under the weak acid condition, the estimated S_{COOH} is 87.87 $Å^2$/ion for KL and 136.19 $Å^2$/ion for OL based on the picked calibration point.

Table S1. Total ionized phenolic groups in 20 mM NH_4HCO_3 and the corresponding estimation of the area per phenolic groups and carboxylic groups in lignin based on a-single-lignin-chain method.

Lignin	Ionized PeOH in 20 mM NH_4HCO_3 (mmol/g)	M1		M2	
		$S_{PeOH, tot}$ ($Å^2$/ion)	$S_{PeOH, pKa\ 7.5}$ ($Å^2$/ion)	$S_{PeOH, pKa\ 10.2}$ ($Å^2$/ion)	$S_{COOH, tot}$ ($Å^2$/ion)
KL	0.4665	64.19	463.50	74.51	863.79
OL	1.0502	116.63	217.63	237.75	652.18

Table S2. Approximate expression of ξ at various distance ranges

Condition	**Distance range**	$\boldsymbol{\xi}$ $(\in (\mathbf{0}, \mathbf{1}))$
C1	$b < \frac{1}{\kappa}$	$\sqrt{nSb\left(\frac{H}{Z}\right)}\left(\in \left(0, \frac{1}{\sqrt{2}}\right)\right)$
C2	$\frac{1}{\kappa} \leq b \leq \frac{\pi}{\kappa}$	$\frac{4}{\pi^2}\left[\frac{\kappa b}{2} + \left(\frac{\kappa}{2nS}\frac{Z}{H}\right)^{-\frac{1}{3}}\right]^2 \left(\in \left(0, \frac{1}{\sqrt{2}}\right)\right)$
C3	$b > \frac{\pi}{\kappa}$	$\frac{\kappa}{nS} e^{-\kappa b}\left\{1 + \left(\frac{H}{Z}\right)\left[\frac{\theta_3\left(0, \frac{\kappa}{8nS}\right) + 1}{\theta_4\left(0, \frac{\kappa}{8nS}\right) + 1}\right]^2\right\}^{-1} \left(\in \left(\frac{1}{\sqrt{2}}, 1\right)\right)$ $\theta_3(0, q) \approx 1 + 2q + 2q^4 + 2q^9$ $\theta_4(0, q) \approx 1 - 2q + 2q^4 - 2q^9$ where $q < 1$

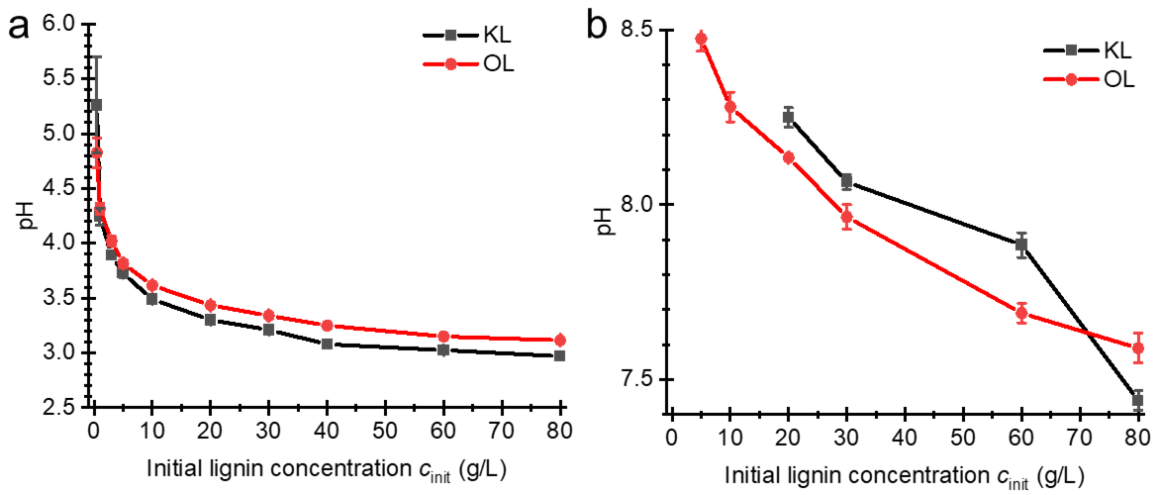

Figure S1. pH of LNPs mixture as the function of the initial lignin concentration c_{int} with (a) DI water and (b) 20 mM NH_4HCO_3 as antisolvent.

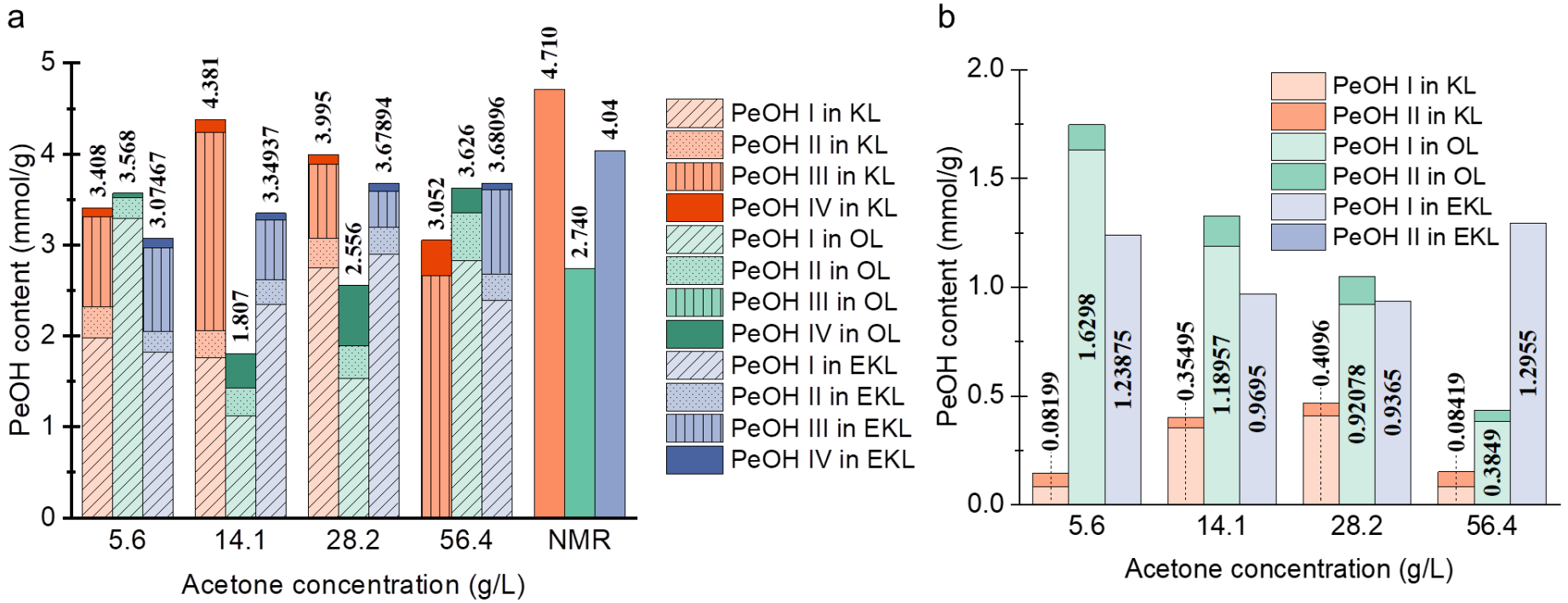

Figure S2. (a) Phenolic hydroxyl group (PeOH) contents measured in different acetone concentration via UV difference method and compared with NMR data. (b) PeOH I and II via UV difference method.

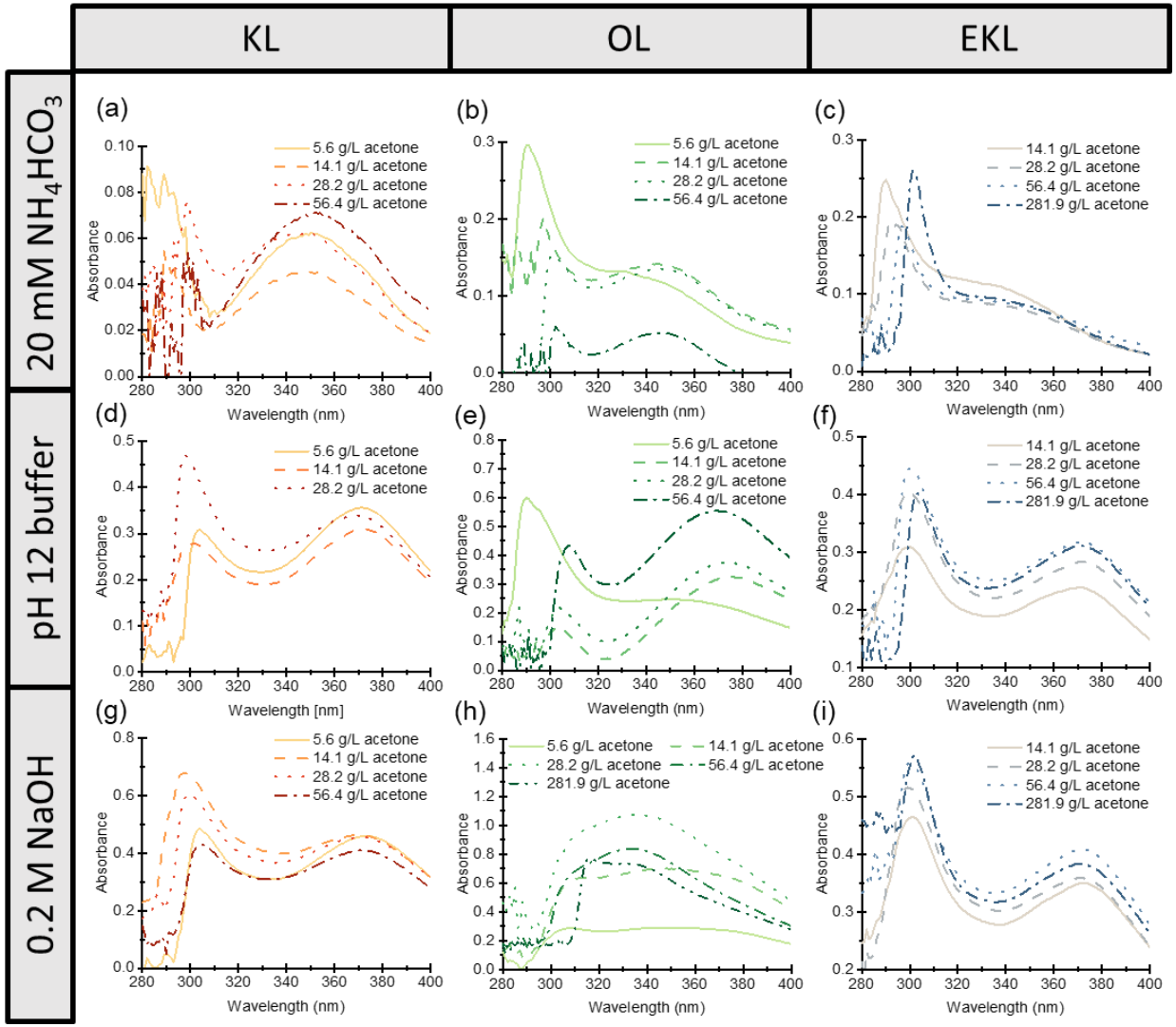

Figure S3. Typical difference UV spectra of (a, d, g) KL, (b, e, h) OL, and (c, f, i) in 20 mM NH_4HCO_3, pH 12 buffer, and 0.2 M NaOH.

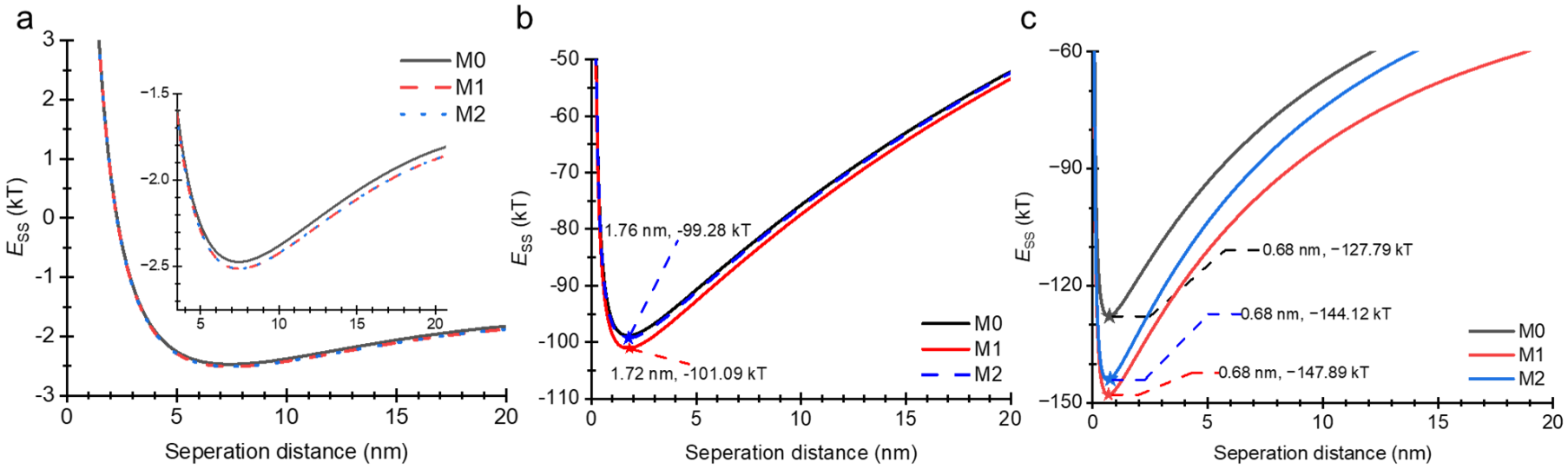

Figure S4. Sphere-sphere interaction energy calculated using different estimation methods of ionizable groups at (a) pH 3.63 and 0.1 mM monovalent salt, (b) pH 5.3 and 0.1 mM monovalent salt between two particles with the same radius of 42 nm; and (c) pH 7.3 and 0.1 mM between two particles with the same radius of 21 nm.

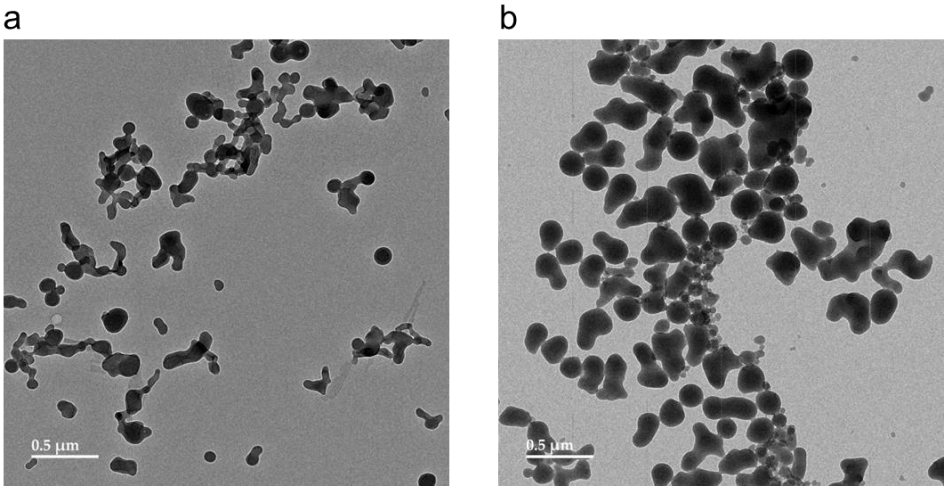

Figure S5. TEM images of (a) OL-NPs and (b) EKL-NPs at c_{init} = 10 g/L and DI water as antisolvent.

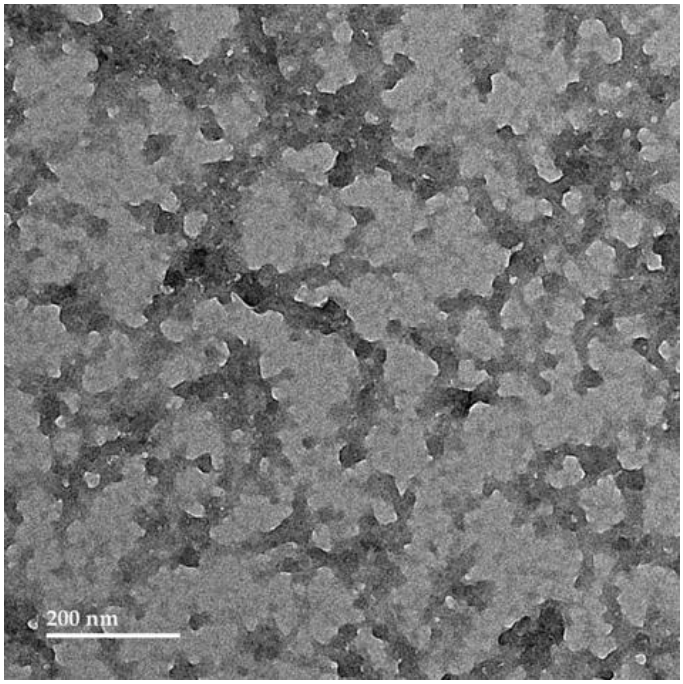

Figure S6. KL-NPs synthesized at c_{init} = 10 g/L and 20 mM NH_4HCO_3 as antisolvent.

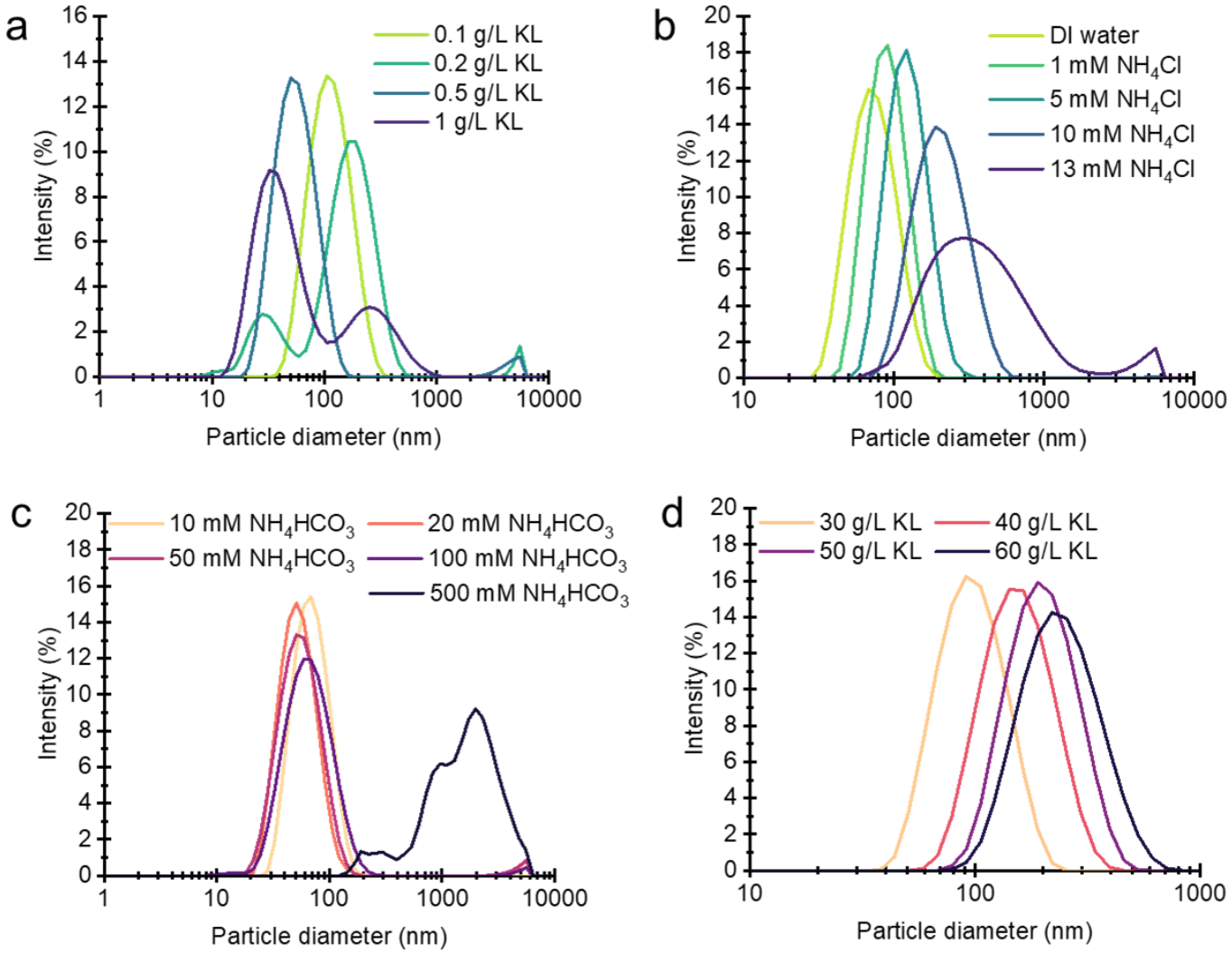

Figure S7. KL-NPs size distribution (a) using 10 mM NH_4Cl as antisolvent at c_{init} = 0.1-1 g/L; (b) using 0-13 mM NH_4Cl as antisolvent at c_{init} = 10 g/L; (c) using 10-500 mM NH_4HCO_3 as antisolvent at c_{init} = 20 g/L; (d) using 20 mM NH_4HCO_3 as antisolvent at c_{init} = 30-60g/L.

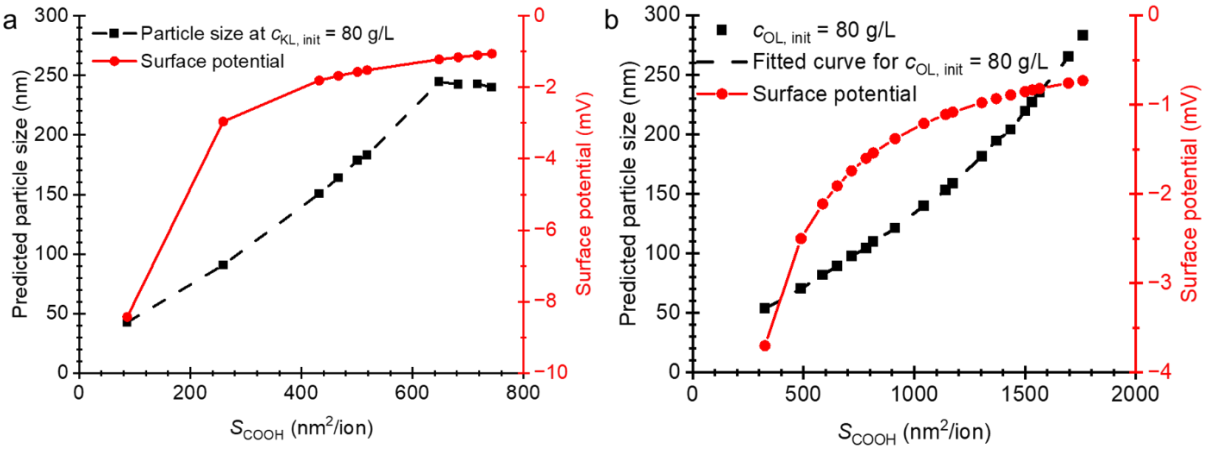

Figure S8. Predicted particle size as the function of S_{COOH} under weak-alkali condition and high initial lignin concentration (c_{init} = 80 g/L) of (a) KL-NPs and (b) OL-NPs.

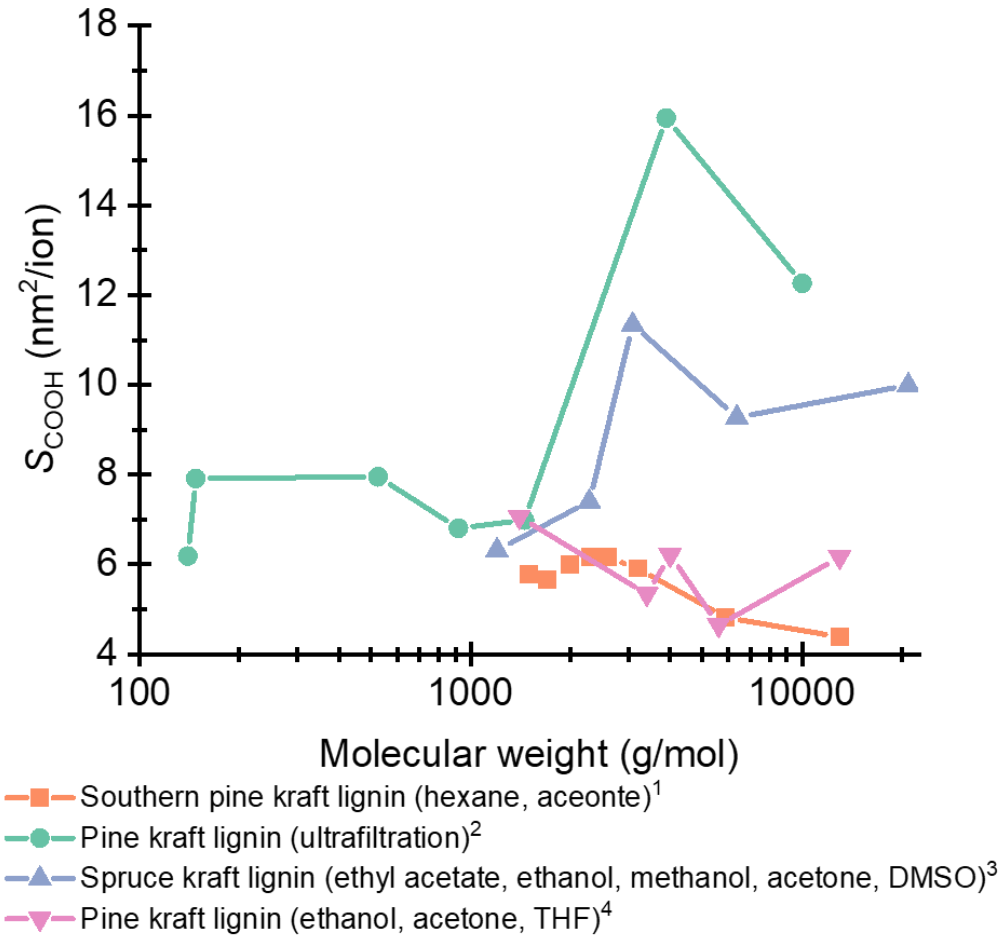

Figure S9. Estimation of area per carboxylic group (S_{COOH}) in lignin based on molecular weight and its corresponding carboxyl group content of the fractionated lignin. ([1]Cui, 2014 [10], [2]Zinovyev, 2017 [11], [3] Pylypchuk, 2021 [12], [4] Zwilling, 2021 [13]).

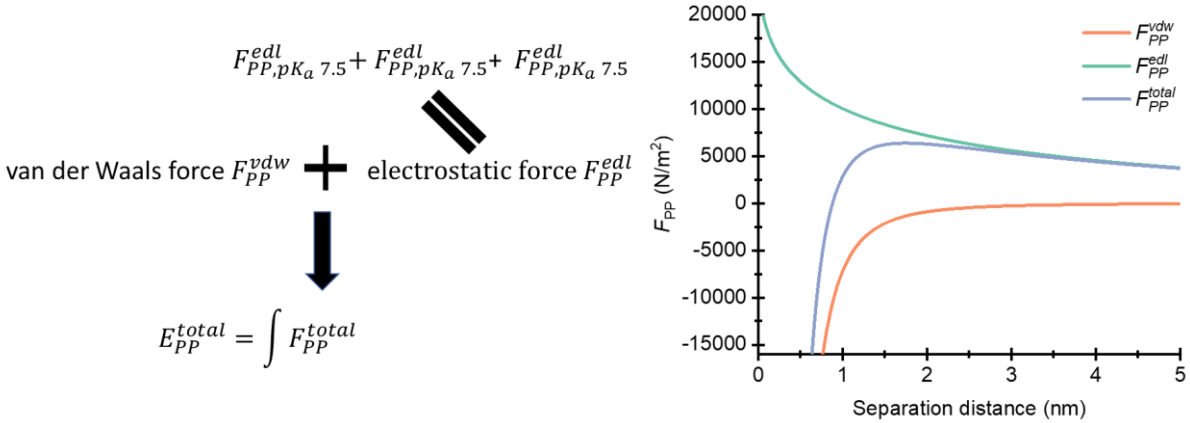

Figure S10. Schematic of the plate–plate force calculation and the example of the interaction force curve with S_{PeOH} = 64.19 Å^2, S_{COOH} = 863.79 Å^2 when pH = 5.3 and salt concentration is 0.1 mM.

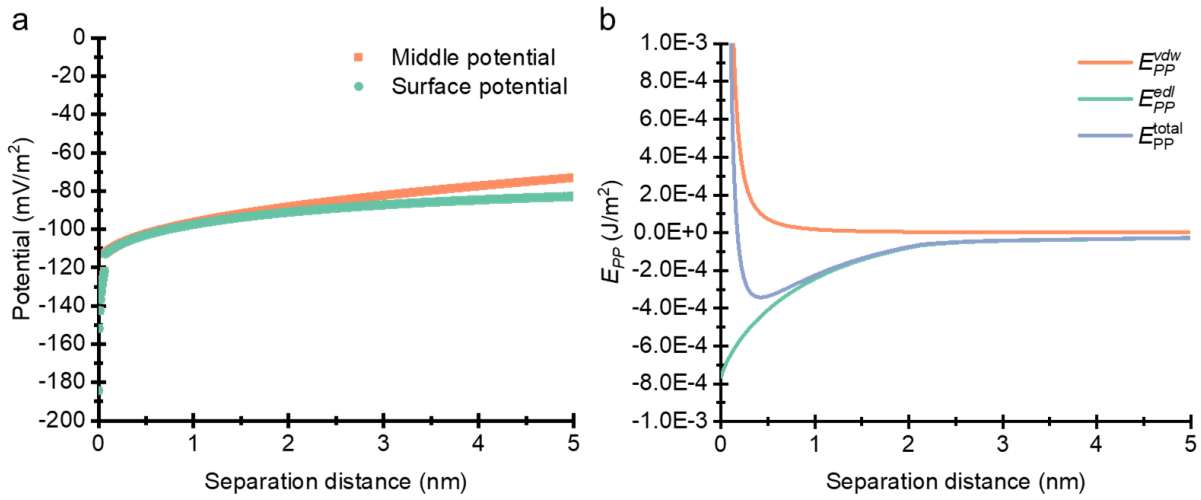

Figure S11. Representative (a) surface potential and (b) interaction energy curve as the function of distance with S_{PeOH} = 64.19 Å^2, S_{COOH} = 863.79 Å^2 at pH 5.3 and 0.1 mM salt concentration.

References

1. X. Meng, C. Crestini, H. Ben, N. Hao, Y. Pu, A. J. Ragauskas and D. S. Argyropoulos, *Nature Protocols*, 2019, **14**, 2627-2647.
2. A. Gärtner, G. Gellerstedt and T. Tamminen, *Nordic Pulp & Paper Research Journal*, 1999, **14**, 163-170.
3. T. Sewring, W. Zhu, M. Sedin and H. Theliander, *Industrial & Engineering Chemistry Research*, 2019, **58**, 3427-3439.
4. S. M. Notley and M. Norgren, *Langmuir*, 2006, **22**, 11199-11204.
5. J. V. Vermaas, L. D. Dellon, L. J. Broadbelt, G. T. Beckham and M. F. Crowley, *ACS Sustainable Chemistry & Engineering*, 2019, **7**, 3443-3453.
6. M. Norgren and B. Lindström, *Holzforschung*, 2000, **54**, 519-527.
7. B. W. Ninham and V. A. Parsegian, *Journal of Theoretical Biology*, 1971, **31**, 405-428.
8. S. Bhattacharjee, M. Elimelech and M. Borkovec, *Croatica Chemica Acta*, 1998, **71**, 883-903.
9. S. Kumar and D. Ramkrishna, *Chemical Engineering Science*, 1996, **51**, 1311-1332.
10. C. Cui, R. Sun and D. S. Argyropoulos, *ACS Sustainable Chemistry & Engineering*, 2014, **2**, 959-968.
11. G. Zinovyev, I. Sumerskii, P. Korntner, I. Sulaeva, T. Rosenau and A. Potthast, *Journal of Wood Chemistry and Technology*, 2017, **37**, 171-183.
12. I. V. Pylypchuk, A. Riazanova, M. E. Lindström and O. Sevastyanova, *Green Chemistry*, 2021, **23**, 3061-3072.
13. J. D. Zwilling, X. Jiang, F. Zambrano, R. A. Venditti, H. Jameel, O. D. Velev, O. J. Rojas and R. Gonzalez, *Green Chemistry*, 2021, **23**, 1001-1012.